Iranian Journal of Materials Forming 8 (3) (2021) 53-66

Online ISSN: 2383-0042

IJMF

Iranian Journal of Materials Forming

Journal Homepage: http://ijmf.shirazu.ac.ir

Research Article

The Comprehensive Study on the Classical Constitutive Models in Predicting the Hot Deformation Behavior of Al5083-SiC Metal Matrix Composite

H. Dalvand and S. Rasaee*

Department of Mechanical Engineering, Faculty of Engineering, Kermanshah University of Technology, Kermanshah, Iran

ARTICLE INFO

Article history:

Received 14 June 2021
Reviewed 4 July 2021
Revised 12 July 2021
Accepted 18 July 2021

Keywords:

Metal matrix composite
Hot deformation
Constitutive equation
Arrhenius model
Johnson-Cook model
Zerilli-Armstrong

ABSTRACT

The main goal of this research is to study the hot deformation process of metal-matrix composites and investigate the possibility of using classical constitutive models to calculate the flow stress of such composites during the hot deformation process. A 5083 aluminum-based metal composite reinforced with 9 wt.% of 37 micron SiC particles, and made by stir-casting method, was used for the study. Standard and improved Johnson-Cook model, Arrhenius and Zerilli-Armstrong models in the temperature range of 673-823 K, and strain rates of 0.001-1 s^{-1} were extracted and their accuracy was studied. Based on the results, classical models used to predict the hot deformation behavior of metal alloys can also be used to predict the behavior of aluminum-matrix composites with reasonable accuracy depending on the type of model. The hot deformation activation energy Q for the composite based on the hyperbolic-sine law Arrhenius equation, is 265.5 kJ/mol. The strain-compensated Arrhenius model was the best model to predict the behavior of the composite with the error less than 7% and can reasonably predict the trend of changing the flow stress even at high temperatures with the correlation factor of 0.989.

1. Introduction

Nowadays, almost all common materials and alloys have been experienced for various uses, and their application limitations have been identified. With an advance in design knowledge, the need for new materials with superior mechanical and physical properties is perhaps the most critical limitation of designers. Hence, there is a constant effort to develop new alloys and materials that can be used in more complicated situations. Among these, metal matrix composites (MMC), which are made by mixing a metallic alloy as a matrix with one or more reinforcing components, have become very important due to their unique properties and the possibility of designing new materials. Aluminum-based composites (AMCs) are one of the most important MMCs that have been vastly applied in the aerospace, automotive, and military industries due to their lightness and high strength. Ceramic particles such as silicon carbide (SiC), alumina (Al_2O_3), graphite, or a combination of these are mainly used as reinforcements to make AMCs. AMC reinforced with SiC particles is one of the most popular types of aluminum-based metal composites due to improved mechanical properties such as

* Corresponding author
E-mail address: rasaee@kut.ac.ir (S. Rasaee)
https://doi.org/10.22099/ijmf.2021.40958.1186

increased strength and abrasion resistance, especially at high temperatures.

Material behavior and the effect of strain rate and temperature on the flow stress of the material and determining the optimal values of the forming process parameters are done by studying the hot compression process of the material [1]. In addition to describing the complex behavior of the material during complex deformation processes, constitutive equations are an essential element in the numerical modeling of these processes. Among the various types of models, phenomenological models are famous for explaining changes in the flow stress of metal materials due to their simplicity, predictability with appropriate accuracy, and the possibility of use in numerical codes. Constitutive models such as Johnson-Cook [2], Arrhenius, and Zerilli-Armstrong are the most popular types of these models, which can be extracted by performing relatively fewer experiments due to their smaller parameters, and due to their high popularity in many commercial finite element software and codes that exist by default and can be used. So far, these models have been widely used to model the hot deformation of many metal alloys, especially aluminum. Ke et al. [3] considered the hot deformation of 7020 aluminum alloy and drew process maps to determine the optimal hot forming parameters of this alloy using the Arrhenius model. Dai et al. [4], studying the hot pressure process of 5083 aluminum alloy, used a model with strain-dependent parameters to predict the flow stress of this alloy during the process and also investigated the metallurgical changes of this alloy. Qian et al. [5] focused on the effect of Mn in 6082 aluminum alloy composition on hot deformation, and in particular on its effect on metallurgical changes in alloy recovery and recrystallization during the process by studying the Zener-Hollomon parameter. He et al. [6] determined the optimal forming parameters of casting 5052 aluminum alloy by using process maps based on Arrhenius model during hot deformation. Sun et al. [7] also determined the optimal range of forming parameters for 6A02 aluminum alloy studying the hot deformation. In a comprehensive study, Chen et al. [1] examined the performance of normal and improved Johnson-Cook and Arrhenius models in predicting the flow stress of 6026 aluminum alloy during hot deformation. Chen et al. [8], presenting a model based on the Arrhenius model to predict the flow stress of 7005 aluminum alloy, also explained the microstructural evolution of this alloy during deformation at high temperatures. Although the study of the hot deformation process of aluminum alloys has been extensive, the study of aluminum-based composites and especially the use of structural models to predict their behavior has been limited. Wang et al. [9] studied the effect of the amount of alumina nanoparticles on the deformation behavior of Al-12Si aluminum matrix campsite using the Arrhenius model. They also explored the microstructure evolution of the composite as a dynamic softening mechanism during the high-temperature deformation of the composite. Chen et al. [10] studied the metallurgical process of hot deformation of hybrid AMC reinforced with nano-TiB_2 and micro-SiC particles and the ability to identify the dynamic recrystallization process during hot deformation. They presented a simple structural model based on Arrhenius model for this composite. Narayan et al. [11] studied the ductility of aluminum composite under hot deformation process using strain hardening parameters. Yii et al. [12] studied the recrystallization during hot compression of Al-20%Si composite. Yahu et al. [13] investigated the optimal processing parameters of dual-scale SiCp/A356 composites that were determined to explore the control strategy of the microstructure. Xia et al. [14] studied the deformation and microstructural behaviors of a 20%Al_2O_3-Al6061 composite with a hot torsion test from 25 to 540°C with strain rates of 0.1, 1 and 5 s^{-1}. Kai et al. [15] studied the hot deformation behavior of in-situ 5 wt.% nano ZrB_2/2024Al composite at deformation temperatures of 350-450°C and strain rates of 0.001-10 s^{-1} and specified that the flow stress depends strongly on the deformation temperature and strain rate, and especially exhibits a strain hardening at high temperature and high

strain rate, related to the introduction of nanoparticles.

Despite the advantages of the stir-casting method in making metal-based composites, forming materials made with this method by other conventional forming techniques such as rolling, forging, and machining has limitations and difficulties. Due to the presence of a hard reinforcement in the soft matrix that creates areas with a high stress concentration at the particle location [10], in addition to limiting the composite formability [11], the composite behavior is more sensitive to parameters affecting the process, such as temperature and strain rate during forming processes. In these studies, in addition to determining how the material behavior is affected by process parameters, the constitutive equations governing the material flow stress in terms of strain, temperature, and strain rate can also be extracted and used for numerical modeling of the forming processes of these parts.

2. Experimental Procedure

To make the composite, 5083 aluminum alloy and silicon carbide powder with particle sizes of 10 and 37 µm with a purity of more than 99% have been used. The chemical composition of Al5083 is shown in Table 1.

Since the parameters of particle size and their amount in the composition can have an important influence on the mechanical properties of the final product [10, 12], first, by designing and analyzing experiments, the effect and optimal values of the parameters to achieve a composite with the highest compressive strength have been determined. For this purpose, by selecting the values of 3, 6, 9 and 12 wt.% of SiC powder and particles with sizes of 10 and 37 microns, composite composition optimization tests have been designed using the Taguchi test design method (Table 2). To make the composite, the stir-casting method has been used. In this process, aluminum melt is prepared in a furnace and after adding preheated SiC particles, the mixture is stirred using a stirrer at a constant speed to disperse the particles in the matrix. Although this method is simple and does not require much-advanced equipment, it is necessary to control parameters such as melt temperature and temperature during stirring, stirring time, stirrer height inside the melting chamber, and raising the melt temperature after stirring [16-18].

After making the composite, samples for pressure test according to ASTM E9 standard have been prepared. The tested samples were cylindrical with a diameter of 8 mm and a height of 12 mm. To prevent buckling during the pressure test, the ratio of height to diameter is 1.5. Table 2 lists the test specifications and the result of the pressure test for each sample. The test results are based on Taguchi theory and analyzed in Minitab statistical analysis software environment. Based on the results, the sample with 37 micron reinforcing particles showed

Table 1. Chemical composition of the used aluminum alloy

Al5083	Composing elements (wt.%)								
	Ti	**Zn**	**Cr**	**Mg**	**Mn**	**Cu**	**Fe**	**Si**	**Al**
	0.15	0.25	0.15	4.49	0.65	0.1	0.4	0.4	Balanced

Table 2: Compressive stress test results

S. No	wt.%	Size (µm)	Compressive strength (MPa)
1	3	37	1454.4
2	3	10	1462.7
3	6	37	1355.5
4	6	10	1491.3
5	9	37	1566.6
6	9	10	1546.5
7	12	37	1302.6
8	12	10	1101.6

better behavior in all samples and the best percentage of reinforcement that can be added to the base material to withstand more compressive stress is 9 wt.%. Also, according to the results, the effect of particle size on compressive strength was more remarkable.

To ensure uniform distribution of particles in the matrix, the fabricated composites were explored using metallographic methods. An example (related to sample number 8) is shown in the Fig. 1(a). As shown in the figure, the distribution of powder particles in the matrix was appropriate and relatively uniform. Additionally, to create a uniform microstructure in the samples and eliminate the effects of the manufacturing stage, especially work hardening, the samples have been homogenized and heat-treated at 770 K for 12 h and then cooled, in agreement with the ASTM B917 standard. The initial microstructure of the specimens is shown in Fig. 1(b).

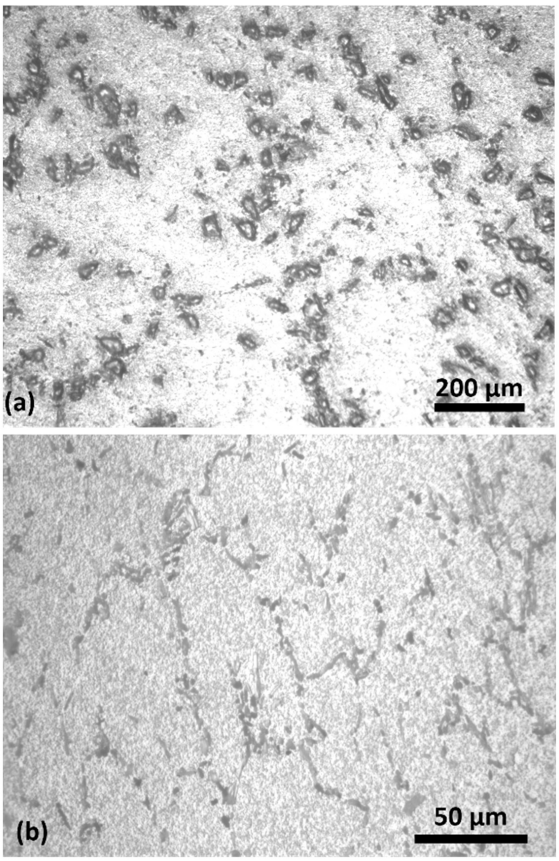

Fig. 1. The cross-section image of the prepared samples with magnification: (a) the distribution of SiC Particles in the Aluminum matrix, (b) Microstructure of the matrix.

After making the composite with the optimal composition, according to ASTM-E9 standard, cylindrical specimens with the height of 12 mm and the diameter of 8 mm were prepared using a machining process (Fig. 2(a)). The tests were done in the temperature range of 673-823 K, with 50-degree steps, and at a strain rate of 0.001 to 1 s^{-1}. To perform hot compression tests, the servo-electric SANTAM STM-150 machine was used, which is equipped to perform tensile and compressive tests at high temperatures and strain rates. After placing the sample in the machine and reaching the furnace temperature to the test temperature, a 5-minute delay was performed to ensure the homogeneous temperature distribution all over the sample, then the test was started and continued until the sample reached a strain of about 0.6. A schematic of the test steps is shown in Fig. 2(b).

3. Results and Discussion

In modeling bulk metal forming processes such as extrusion or rolling, which are mainly performed at high temperatures with high plastic strains, a structural model

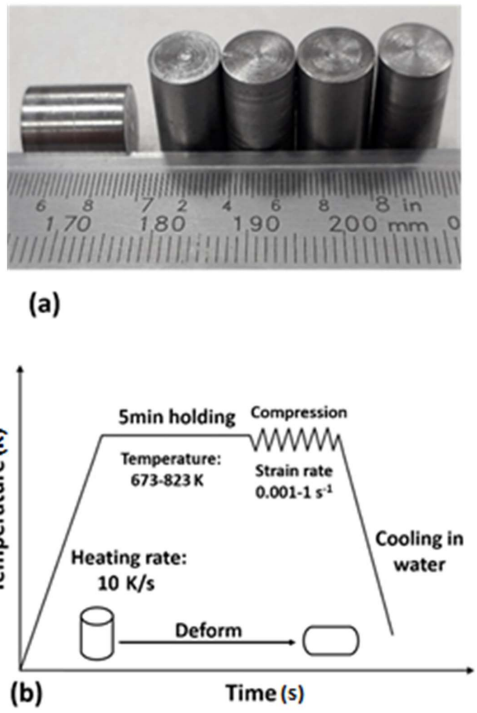

Fig. 2. (a) Standard compression samples, (b) the schematic diagram of the test.

that can predict material flow stress at elevated temperatures and different strain rates is essential. Based on a constitutive model, flow stress depends on temperature parameters, strain rate and strain using mathematical functions, the function and constants of which are determined by observations of experimental results. So far, various models have been presented and the most common one has been used in this research.

The true stress-strain curves attained from the composite hot pressure test are shown in Fig. 3. The process of change is almost the same in all conditions. In the primary stage, the stress rises rapidly by increasing the strain, which may be related to the work hardening phenomenon [19]. Then, the stress reaches a maximum and then remains almost constant as the strain increases. Furthermore, the stress has increased in almost all conditions with a slight slope, which can indicate the dominance of work hardening over the phenomenon of dynamic softening [20]. Because the stress-strain curve for a material undergoing dynamic recrystallization generally has a broad peak, and for materials undergoing only dynamic recovery, the curve has a stress-increasing region followed by a planar region (constant stress), and a peak is not observed in the diagram [21], it can be inferred that dynamic recovery is the rate-controlling mechanism during the hot deformation process.

3.1. Normal Johnson-Cook Model

Johnson-Cook model (JC) considers the effects of work-hardening, strain rate and thermal softening in predicting the flow stress. In this model, the effect of strain, strain rate and deformation temperature on flow stress are given in separate expressions in the multiplicative form. In other words, this model accepts that work-hardening and the rate of it, and the thermal softening are independent and can be separated. This model cannot show any of the effects of thermal history and strain rate [2]. The JC model is expressed mathematically as follows:

$$\sigma = (A + B\varepsilon^{n})(1 + C\ln\dot{\varepsilon}^{*})(1 - T^{*m}) \quad (1)$$

In this model, each of the relationships in parentheses to the right of the Eq. (1) are used to define the effects of work-hardening, strain rate and temperature, respectively. More precisely, the first part expresses the effect of strain on flow stress, the second part describes

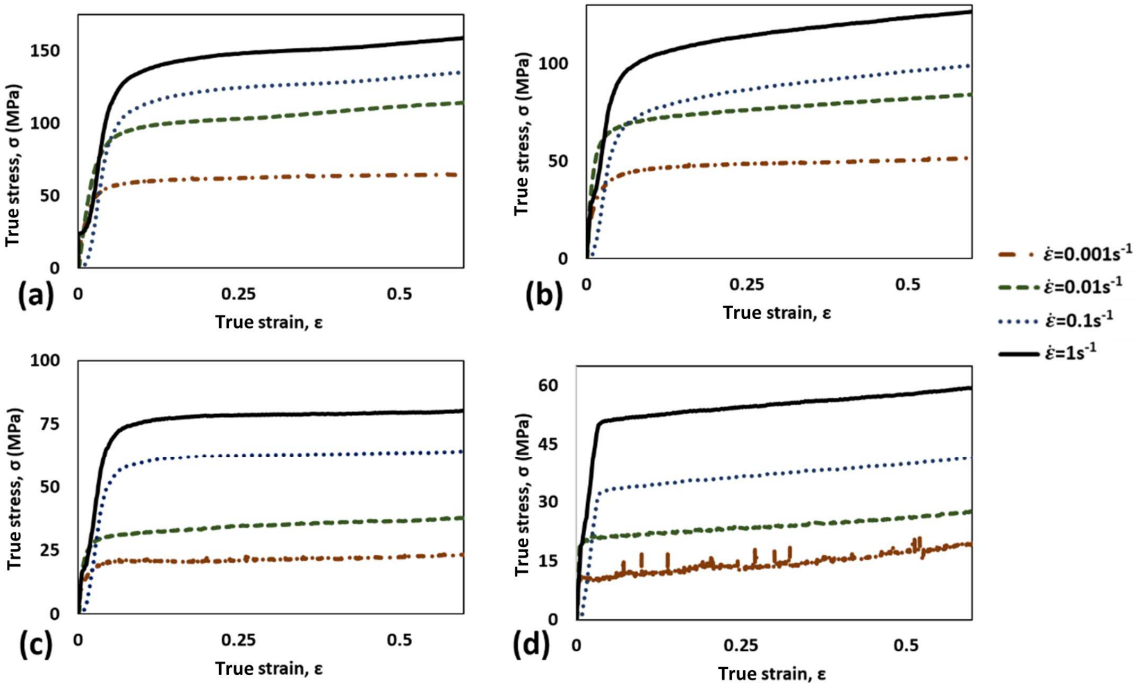

Fig. 3. The true stress-strain curve of the prepared composite at: (a) 673 K, (b) 723 K, (c) 773 K, and (d) 823 K.

the sensitivity to strain rate and the third expresses the dependence of temperature on strain rate. The value of constant A is equal to the yield stress in the reference conditions and the calculated value for it is equal to 59.8 MPa.

By simplifying the basic equation at the reference conditions, the flow stress is expressed as follows:

$$\sigma = A + B\varepsilon^n \quad (2)$$

The constants n and B are the slope and intercept of the line that is fitted on the $\ln(A-\sigma) - \ln\varepsilon$ data, respectively, which are plotted in Fig. 4(a), and their values are n = 0.9074 and B = 7.34 MPa.

At the reference temperature, the Johnson-Cook equation is simplified as follows:

$$\frac{\sigma}{A+B\varepsilon^n} = 1 + C\ln\dot{\varepsilon}^* \quad (3)$$

Then, if at the reference temperature and at various strain rates, the flow stresses measured at different strains are arranged and a line with intercept 1 fitted on data $\frac{\sigma}{A+B\varepsilon^n}$ in terms of $\ln\dot{\varepsilon}^*$, as shown in Fig. 4(b), then the material C constant that will be the slope of this line, is calculated to be equal to 0.2. Also, at the reference strain rate, the JC equation can be rewritten as follows:

$$\frac{\sigma}{A+B\varepsilon^n} = 1 - T^{*m} \quad (4)$$

On data $\ln[1-\sigma]/(A+B\varepsilon^n)]$ in terms of $\ln T^*$ at the reference strain rate and temperatures of 450, 500 and 550 K, and at strains in the range of 0.1 to 0.6, a line is fitted with intercept 0 (Fig. 4(c)) that the slope of this line is the constant m which is equal to m = 0.9618.

Finally, after extracting all the constants, the standard JC model for the composite is summarized as follows:

$$\sigma = (59.8 + 7.34\,\varepsilon^{0.9074})(1 + 0.2101\,\ln\dot{\varepsilon}^*)(1 - T^{*0.9618}) \quad (5)$$

3.2. Modified Johnson-Cook Model

To overcome the shortcoming of assuming the effect of strain, strain rate and temperature on the hot deformation independently in the standard JC model, Lin et al. [22] suggested a modified model based on the standard JC, which significantly improves the prediction accuracy. The modified JC model is expressed as follows:

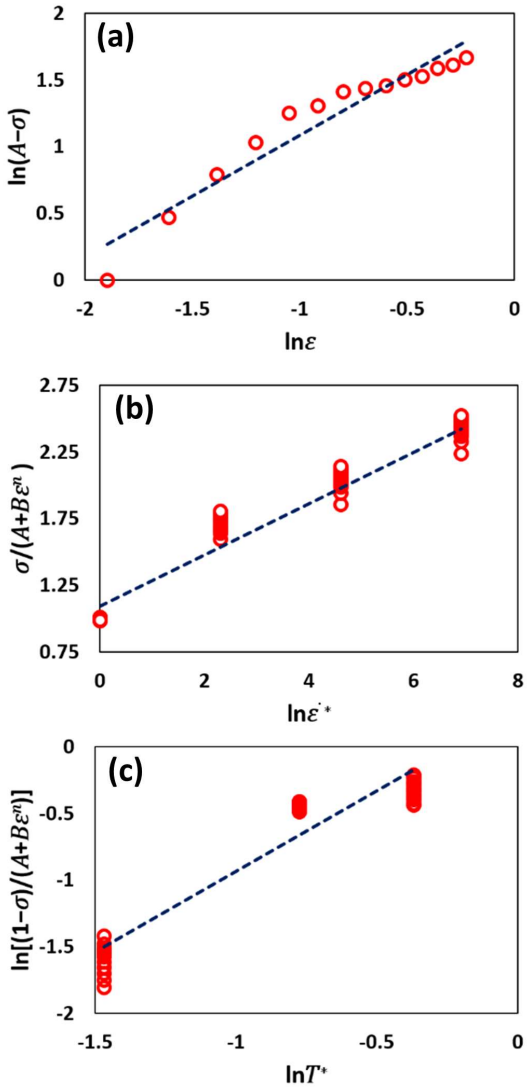

Fig. 4. Collection of figures related to the Johnson-Cook model, (a) $\ln(A-\sigma) - \ln\varepsilon$, (b) $\frac{\sigma}{A+B\varepsilon^n} - \ln\dot{\varepsilon}^*$, and (c) $\ln[(1-\sigma)/(A+B\varepsilon^n)] - \ln T^*$.

$$\sigma = (A_1 + B_1\varepsilon + B_2\varepsilon^2)(1 + C_1\ln\dot{\varepsilon}^*)\exp[(\lambda_1 + \lambda_2\ln\dot{\varepsilon}^*)(T - T_r)] \quad (6)$$

This equation is simplified in the reference conditions as follows:

$$\sigma = A_1 + B_1\varepsilon + B_2\varepsilon^2 \quad (7)$$

Using true stress-strain data in reference conditions, if a quadratic equation fitted on the data σ in terms of ε as shown in the Fig. 5(a), the values of the constants A_1, B_1, B_2 are calculated: A_1=58.501, B_1=16.627, and B_2=-10.983.

This model at the reference temperature is written as follows:

$$\sigma = (A_1 + B_1\varepsilon + B_2\varepsilon^2)(1 + C_1 \ln \dot{\varepsilon}^*) \quad (8)$$

If a line with intercept 0 is fitted on the data $\sigma/(A_1 + B_1\varepsilon + B_2\varepsilon^2)$ in terms of $\ln \dot{\varepsilon}^*$ at the reference temperature, as shown in Fig. 5(b), then the slope of this line will be equal to the constant C, which is equal to 0.2199.

If the expression $(\lambda_1 + \lambda_2 \ln \dot{\varepsilon}^*)$ is replaced by the parameter λ in Eq. (6), then the equation can be rewritten as follows:

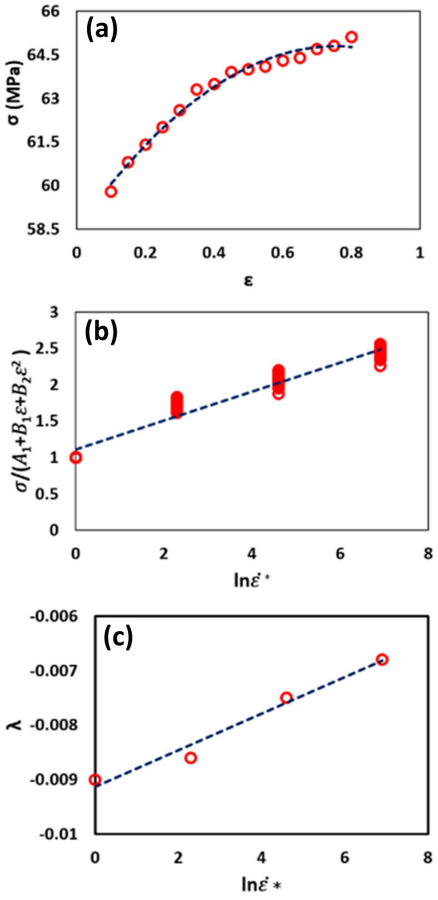

Fig. 5. Collection of figures related to the Modified Johnson-Cook model, (a) $\sigma - \varepsilon$, (b) $\frac{\sigma}{(A_1+B_1\varepsilon+B_2\varepsilon^2)} - \ln \dot{\varepsilon}^*$, (c) λ-ln $\dot{\varepsilon}^*$.

$$\ln[\sigma/(A_1 + B_1\varepsilon + B_2\varepsilon^2)(1 + C_1 \ln \dot{\varepsilon}^*)] = \lambda(T - T_r) \quad (9)$$

In the above statement, all the constants to the left of the equation have already been calculated. If at any strain rate the data $\ln[\frac{\sigma}{A_1+B_1\varepsilon+B_2\varepsilon^2}]$ are plotted in terms of $(T - T_r)$ and a line with intercept 0 matches them, then λ will be the slope of this line for that strain rate, the results are given in Table 3. If the values of λ are obtained at any strain rate and then a line is fitted on the to the data λ in terms of $\ln \dot{\varepsilon}^*$, then λ_1 and λ_2 will be the intercept and the slope of this line (Fig. 5(c)), respectively, which are equal to λ_1=-0.0091 and λ_2=0.0003.

Table 3. Values of λ at different strain rates

Strain rate (s^{-1})	0.001	0.01	0.1	1
λ	-0.009	-0.0086	-0.0075	-0.0068

Finally, the modified JC model equation, which is governing the hot deformation behavior of this composite, is presented as follows:

$$\sigma = (58.501+16.627\varepsilon\text{-}10.983\varepsilon^2)(1 + 0.2199 \ln \dot{\varepsilon}^*) \exp[(-0.0091+0.0003 \ln \dot{\varepsilon}^*)(T - T_r)] \quad (10)$$

3.3. Arrhenius Model

Arrhenius model has an acceptable accuracy in predicting the flow stress, especially at high deformation temperatures [23]. Depending on the level of material flow stress, different mathematical equations are used to define the relation between process parameters (temperature, strain rate and strain) and flow stress [24]. The hyperbolic-sine equation is suitable for a wide range of stresses and is expressed as follows:

$$\dot{\varepsilon} = A\,[\sinh(\alpha\sigma)]^n \exp(-\frac{Q}{RT}) \quad (11)$$

In addition, the effect of strain rate and temperature on the hot deformation behavior of the material can be formulated using the Zener-Hollomon (Z) parameter as follows [25]:

$$Z = \dot{\varepsilon} \exp\left(\frac{Q}{RT}\right) \quad (12)$$

Using the Zener parameter, the relation of material flow stress according to Arrhenius model can be expressed as follows:

$$\sigma = \frac{1}{\alpha} \ln\left\{\left(\frac{Z}{A}\right)^{1/n} + \left[\left(\frac{Z}{A}\right)^{2/n} + 1\right]^{1/2}\right\} \quad (13)$$

If the data $\ln\sigma$ and σ are plotted in terms of $\ln\dot{\varepsilon}$ and lines are matched to these data (Fig. 6(a) and (b)) respectively, and the slope of these lines is calculated, then the value of α will be calculated by dividing the slope of the first line by the second, which was equal to 0.01947.

The activation energy Q is also calculated from the following equation, in which $\left[\frac{\partial \ln\dot{\varepsilon}}{\partial \ln[\sinh(\alpha\sigma)]}\right]_T$ is the inverse of the slope of the line fitted on the data $\ln[\sinh(\alpha\sigma)]$ in term of $\ln\dot{\varepsilon}$ at constant temperature (Fig. 6(c)) and $\left[\frac{\partial \ln[\sinh(\alpha\sigma)]}{\partial(1/T)}\right]_{\dot{\varepsilon}}$ is the slope of the line fitted the data of $\ln[\sinh(\alpha\sigma)]$ in term of $(1/T)$ at constant strain rate, (Fig. 6(d)).

$$Q = R\left[\frac{\partial \ln\dot{\varepsilon}}{\partial \ln[\sinh(\alpha\sigma)]}\right]_T \left[\frac{\partial \ln[\sinh(\alpha\sigma)]}{\partial(1/T)}\right]_{\dot{\varepsilon}} \quad (14)$$

As stated by Eq. (14) the activation energy Q, of this composite is 265.5 kJmol^{-1} which is much higher than the value of pure aluminum 142 kJmol^{-1} [26], which could indicate the presence of dynamic recrystallization as a dominant mechanism in microstructural evolutions. If the value of Z is calculated from Eq. (12) and their corresponding values of $\ln[\sinh(\alpha\sigma)]$ are also obtained, then the slope and intercept of the line which is fitted on the data of $\ln Z$ in terms of $\ln[\sinh(\alpha\sigma)]$ will be equal to the values of n and A, respectively (Fig. 7). In this research, the values of n and A are calculated as 4.5029 and 3.41657×10^{16}, respectively.

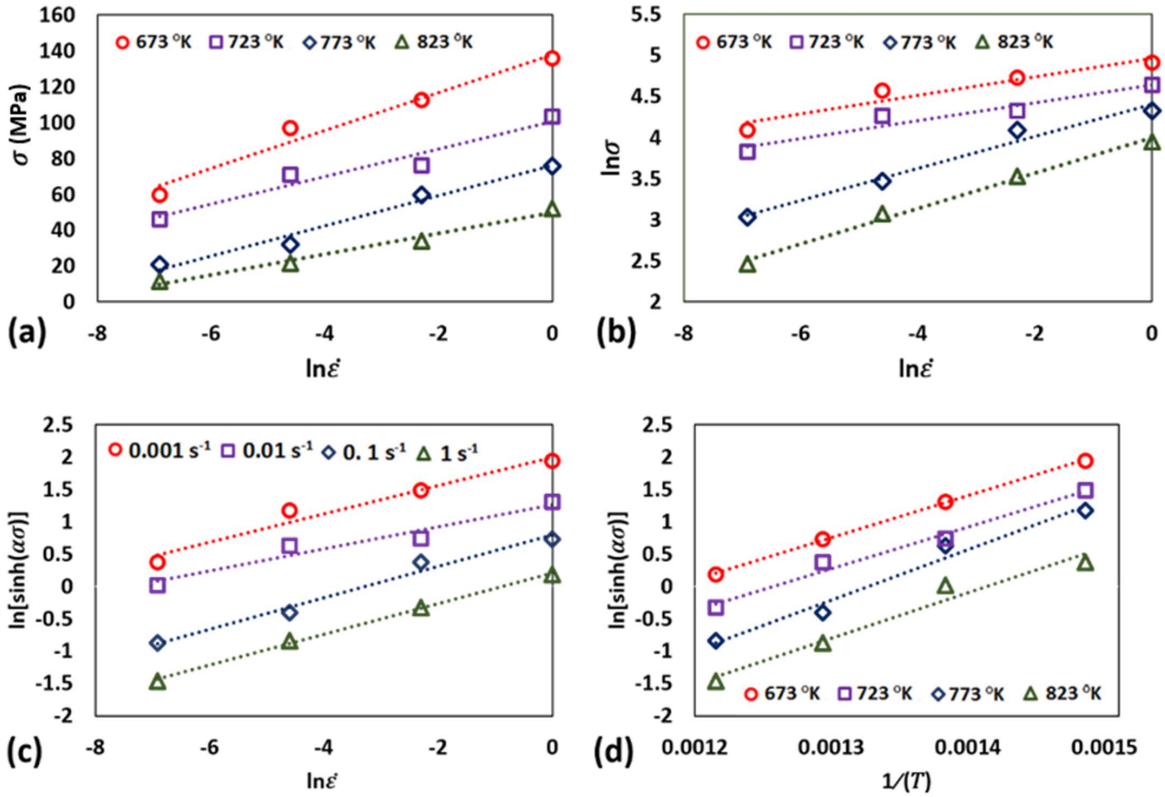

Fig. 6. Collection of figures related to the Arrhenius model, the relations between (a) $\sigma - \ln\dot{\varepsilon}$, (b) $\ln\sigma - \ln\dot{\varepsilon}$, (c) $\ln[\sinh(\alpha\sigma)] - (1/T)$, and (d) $\ln[\sinh(\alpha\sigma)] - \ln\dot{\varepsilon}$.

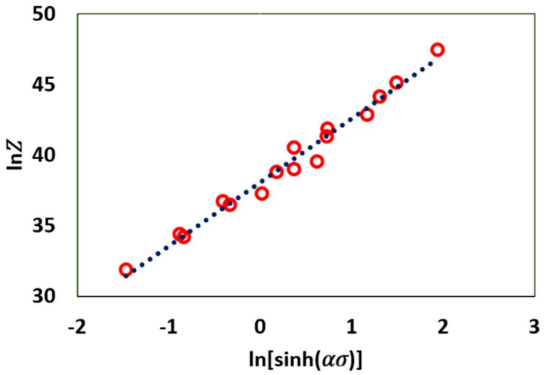

Fig. 7. The relations between $\ln[\sinh(\alpha\sigma)]$ and $\ln Z$.

Finally, after the above analysis, the Arrhenius model for the composite studied in this study is as follows:

$$\sigma = \frac{1}{0.01947}\ln\left\{\left(\frac{Z}{3.41657\times10^{16}}\right)^{1/4.5029} + \left[\left(\frac{Z}{3.41657\times10^{16}}\right)^{2/4.5029} + 1\right]^{1/2}\right\} \quad (15)$$

3.4. Arrhenius strain compensation model

It should be noted that in the Arrhenius model the effect of strain is not considered. However, as shown in the figure, the deformation activation energy and the constant of the material are meaningfully affected by the strain. Usually, flow stress is variable in terms of strain, especially due to dynamic recrystallization which can significantly reduce the flow stress. Therefore, the Arrhenius model may be unsuitable to describe the dynamic softening phenomenon. To provide a more accurate prediction of flow stress, strain compensation must be included in the Arrhenius model. The constants of materials under different strains from 0.05 to 0.5 with an interval of 0.05 were calculated by the method explained in the previous section and the results are plotted in the Fig. 8(a)-(d).

It can be seen that the effect of strain on the material constant in the whole strain range is significant. The fifth-order polynomial equations can be used with sufficient accuracy to describe the relation between strain and the constants of material, as shown in Eq. (16). The results are presented in Table 4:

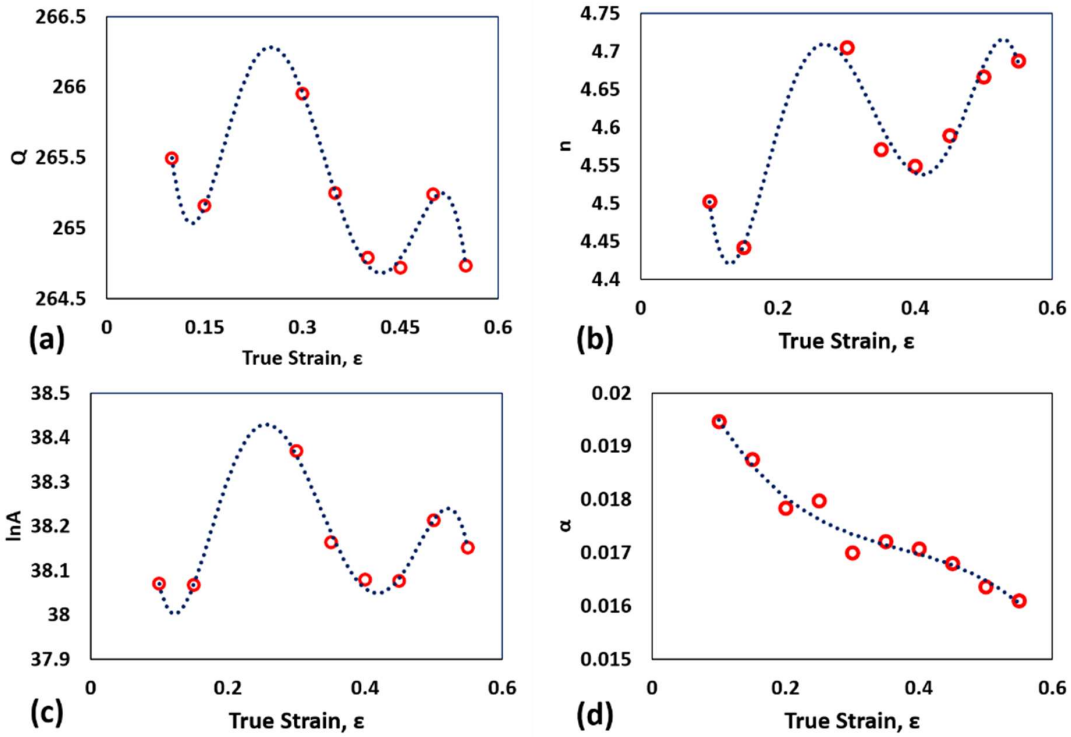

Fig. 8. Collection of figures related to the Arrhenius strain compensation model, the relations between (a) Q, (b) n, (c) $\ln A$, (d) α and true strain ε.

$$\alpha = B_0 + B_1\varepsilon + B_2\varepsilon^2 + B_3\varepsilon^3 + B_4\varepsilon^4 + B_5\varepsilon^5$$
$$n = C_0 + C_1\varepsilon + C_2\varepsilon^2 + C_3\varepsilon^3 + C_4\varepsilon^4 + C_5\varepsilon^5$$
$$Q = D_0 + D_1\varepsilon + D_2\varepsilon^2 + D_3\varepsilon^3 + D_4\varepsilon^4 + D_5\varepsilon^5 \quad (16)$$
$$\ln A = E_0 + E_1\varepsilon + E\varepsilon^2 + E\varepsilon^3 + E_4\varepsilon^4 + E_5\varepsilon^5$$

Table 4. Polynomial coefficients describing material coefficients

α	Q	n	ln *A*
B_0=0.0196	C_0=283.23	D_0=7.6144	E_0=42.187
B_1=0.0208	C_1=-400.38	D_1=-69781	E_1=-95719
B_2=-0.340	C_2=3197.7	D_2=550.41	E_2=785.03
B_3=1.4117	C_3=-11411	D_3=-1929.8	E_3=-2831.4
B_4=-2.4212	C_4=18608	D_4=3096	E_4=46346
B_5=1.484	C_5=-11312	D_5=-1853.8	E_5=-2815.6

3.5. Modified Zerilli–Armstrong model

The modified Zerilli-Armstrong model (ZA) is usually used to estimate the flow stress of materials at high temperatures. The mathematical formula of this model is as follows:

$$\sigma = (C_1 + C_2\varepsilon^n)exp[-(C_3 + C_4\varepsilon)T^* + (C_5 + C_6T^*)\ln\dot{\varepsilon}^*] \quad (17)$$

The Eq. (17) is simplified at the reference strain rate as follows:

$$\sigma = (C_1 + C_2\varepsilon^n)\exp[-(C_3 + C_4\varepsilon)T^*] \quad (18)$$

If the $\ln\sigma$ data are extracted and arranged in terms of strain (in the strain range 0.1-0.6 with steps 0.05) at the temperatures 673-823 K, then in the above expression the values $S_1 = -(C_3 + C_4\varepsilon)$ and $l_1 = \ln(C_1 + C_2\varepsilon^n)$ can be attained from the slope and intercept of the line which is fitted on the $\ln\sigma$ data in term of T^* (Fig. 9(a)); by taking the natural logarithm from both sides of these relations, these expressions are rewritten as follows:

$$\ln(\exp l_1 - C_1) = \ln C_2 + n\ln\varepsilon$$
$$S_1 = -(C_3 + C_4\varepsilon) \quad (19)$$

At the reference conditions C_1 is the yield stress and is equal to 59.8 MPa, and by calculating and placing it in Eq. (19) and plotting $\ln(expl_1 - C_1)$ in terms of $\ln\varepsilon$ (Fig. 9(b)), the values of C_2 and n can be calculated, and their values were equal to 8.158 and 0.0166, respectively. By calculating the values of C_1, C_2 and n, if the S_1 data are plotted in terms of ε (Fig. 9(c)), then C_3 and C_4 will be the slope and intercept of the which is fitted on this data, and their values were equal to 0.012

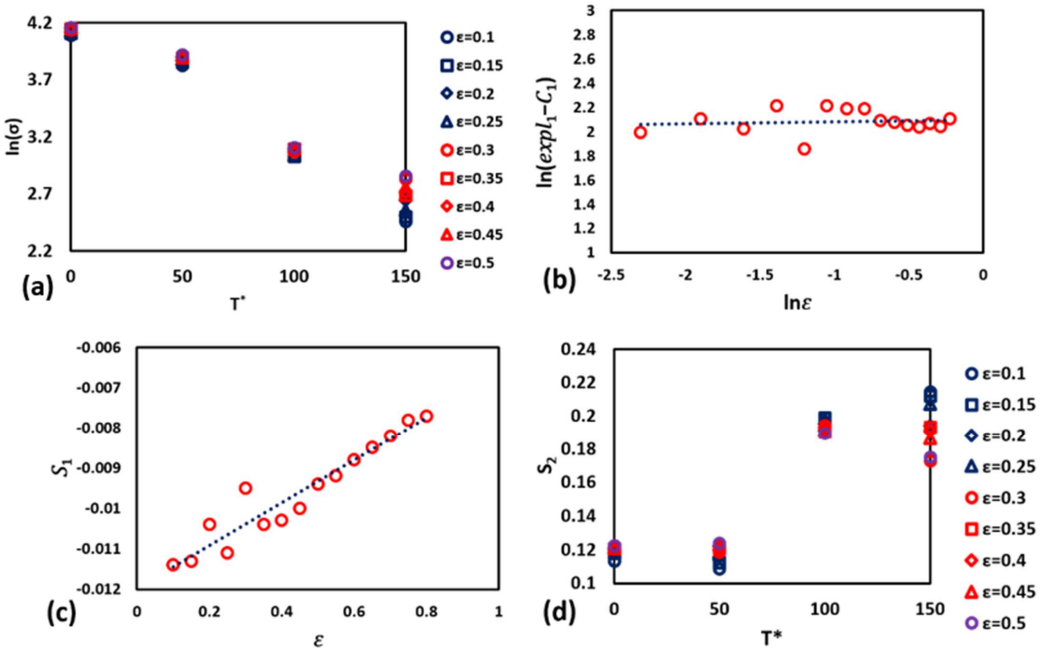

Fig. 9. Collection of figures related to the Modified Zerilli–Armstrong model, the relations between (a) $\ln(\sigma) - T^*$, (b) $\ln(expl_1 - C_1) - \ln\ \varepsilon$, (c) $S_1 - \varepsilon$, (d) $S_2 - T^*$

and -0.0053, respectively. By taking the natural logarithm from the sides of Eq. (17), the following equation is attained, which is used to calculate other constants:

$$\ln\sigma = \ln(C_1 + C_2\varepsilon^n) - (C_3 + C_4\varepsilon)T^* + (C_5 + C_6T^*)\ln\dot{\varepsilon}^* \quad (20)$$

If data $\ln\sigma - \ln\dot{\varepsilon}^*$ are plotted, then the slope of the line fitted on this data will be equal to $S_2 = C_5 + C_6T^*$, which will be a value for this slope for each operating temperature.

Thus, a set of slope values are obtained at various strains and temperatures. If the calculated values of S_2 are plotted in terms of T^* (Fig. 9(d)), then the values of C_5 and C_6 can be obtained from the slope and intercept of the line fitted on these data, and their values would be equal to 0.1169 and 0.000048, respectively.

Finally, all the constants of the modified ZA model are calculated according to the described process, and the proposed modified ZA model for this composite is obtained according to the Eq. (21).

$$\sigma = \left(59.8+8.158\varepsilon^{0.0166}\right)exp\left[-(0.012-0.0053\varepsilon)T^* + (0.1169+0.00048T^*)\,ln\,\dot{\varepsilon}^*\right] \quad (21)$$

3.6. Accuracy analysis of the proposed models

It is necessary to explore the accuracy of the models and determine their accuracy in predicting the amount of flow stress and the trend of its changes after extracting the models describing flow stress in terms of temperature, strain rate and strain. For this purpose, standard qualitative and quantitative statistical comparison methods have been used. The measured flow stress and its corresponding predicted values by different models are plotted in Fig. 10. To quantitatively evaluate

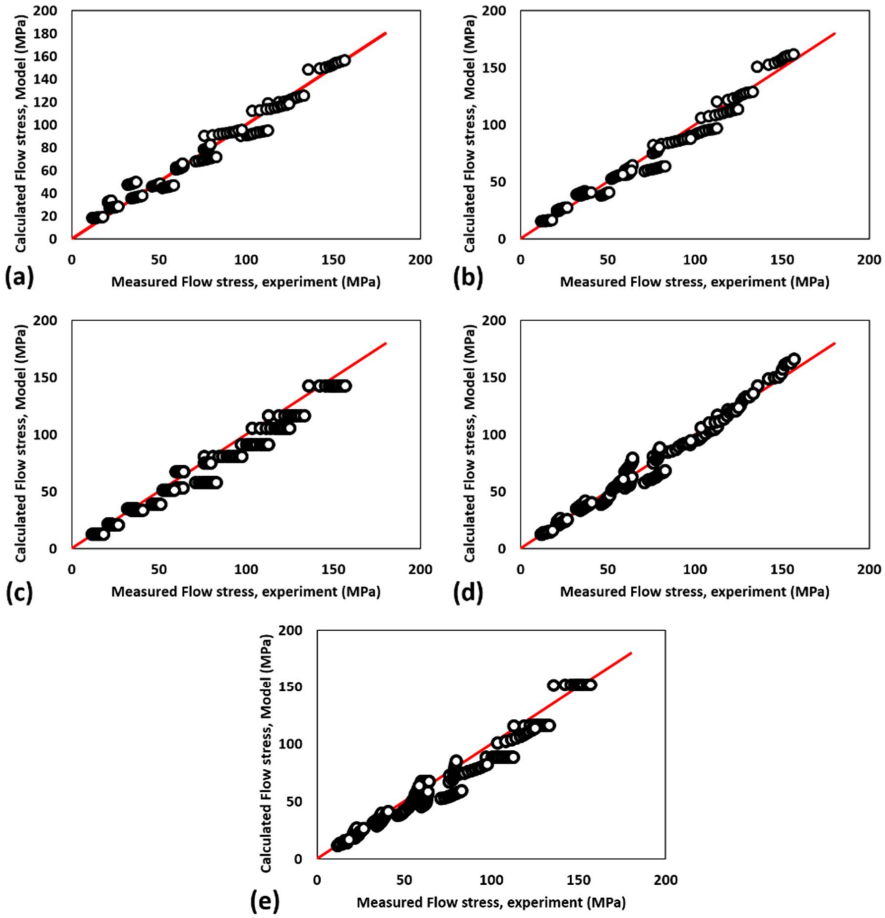

Fig. 10. Comparison between measured flow stresses and calculated from: (a) Johnson-Cook Model, (b) Modified Johnson-Cook Model, (c) Arrhenius model, (d) Arrhenius strain compensation model, and (e) Modified Zerilli–Armstrong model.

the accuracy of the extracted structural models, correlation coefficient (R) and average absolute relative error (AARE) have been used. The correlation coefficient R indicates the ability of the model to predict the trend of changes in experimental and calculated data, and AARE is an unbiased statistical parameter utilized to confirm the prediction accuracy of the models. They are calculated according to the following equations:

$$R = \frac{\sum_{i=1}^{N}(E_i - \bar{E})(P_i - \bar{E})}{\sqrt{\sum_{i=1}^{N}(E_i - \bar{E})^2 \sum_{i=1}^{N}(P_i - \bar{P})^2}}$$
$$AARE\ (\%) = \frac{1}{N}\sum_{i=1}^{N}\left|\frac{E_i - P_i}{E_i}\right| \times 100 \quad (22)$$

To calculate the R and AARE, all the experimental and calculated flow stresses drawn in Fig. 10 have been used and the results are given in Table 5.

Table 5. Calculated values of R and AARE for different manufacturer models

Models	AARE (%)	R
Johnson-Cook	12.62716	0.984
Modified Johnson-Cook	8.756941	0.986
Arrhenius model	10.32087	0.985
Arrhenius strain compensation model	6.953736	0.989
Zerilli-Armstrong	10.21482	0.979

In general, all the studied models have some accuracy in calculating flow stress during hot deformation, although not all of them have the same accuracy rate. Based on the observations of the plotted diagrams (Fig. 10(a)), it is concluded that at high temperatures the accuracy of the JC model was inadequate. But, at low temperatures, with acceptable accuracy, the flow stress was predicted, while in the case of the model in the prediction the trend of changes was not very good (R = 0.9836). The modified Johnson-Cook model (Fig. 10(b)), in addition to better accuracy in predicting flow stress values, could have been more accurate, especially at high temperatures. However, this model has not been much more successful in predicting the trend of change (R = 0.9855). Arrhenius model (Fig. 10(c)) in addition to improving accuracy, in predicting the trend of change was also better than previous models (R = 0.985). Arrhenius strain compensation model, considering the effects of strain (Fig. 10(d)), while having the best accuracy (AARE = 7%) among all models, has been successful in predicting the trend of flow stress changes and has been able to predict the trend of changes with good adaptation (R = 0.989) as shown in Fig. 11; this model has acceptable accuracy in all temperature ranges and strain rates. The Zerilli-Armstrong model (Fig. 10(e)) is only accurate at high

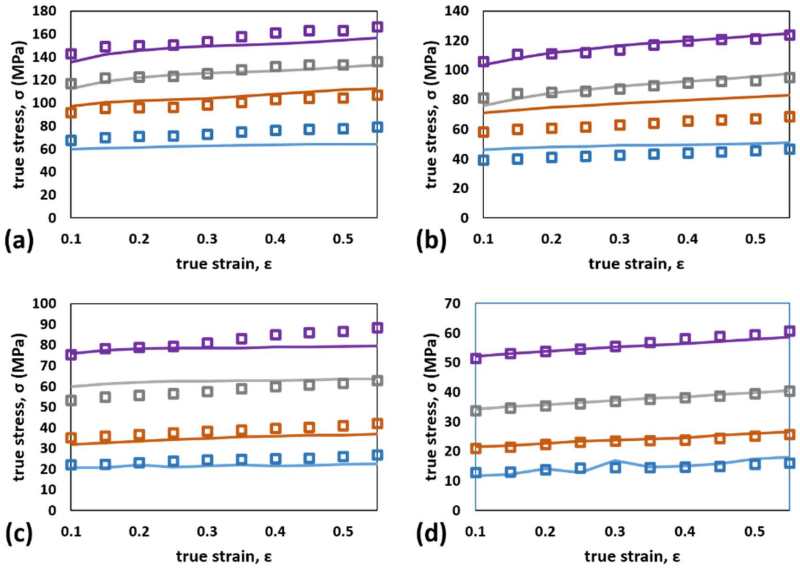

Fig. 11. Comparison between measured flow stresses (Continuous lines) and predicted by Arrhenius strain compensation model (Square symbols): (a) 673 K, (b) 723 K, (c) 773 K, and (d) 823 K.

temperatures and is not recommended in other temperature ranges. Also, this model had the worst accuracy among all the studied models to predict the trend of flow stress changes (R = 0.979).

4. Conclusion

This study investigates the feasibility of using classical constitutive models to calculate the hot deformation behavior of aluminum-based composites. For this purpose, the Al5083-SiC composite was fabricated using the stir-casting method and using Al5083 as a matrix and SiC powder as a reinforcement, its composition was optimized and then by studying the composite hot compression process, different constitutive models were extracted for it. Overall, the achievements of this dissertation can be summarized as follows:

- The Al5083-SiC composite was fabricated using the stir-casting method, the effect of particle size and amount (9 wt. %) of powder on the mechanical properties of the composite was studied and it was found that both parameters have a significant effect on the compression strength of the composite. Using the design and analysis of experiments by the Taguchi method, the effect of the parameters and their optimal values have been studied to find the best composition to achieve a composite with the highest compressive strength.
- The ability of several common constitutive models to predict the behavior of the composite deformation at high temperatures has been studied. In addition to accurately predicting the flow stress in terms of strain, strain rate and temperature, these models should be able to predict the trend of stress changes with these parameters. According to the results, the models can predict the amount of stress with appropriate accuracy, but Arrhenius strain compensation model has the best performance in both predicting the amount and predicting the trend of change.
- The value of hot deformation activation energy Q, which is calculated for the composite based on the Arrhenius model, is 265.5 kJmol^{-1} that increases compared to the value for the 5083 alloy.

Nomenclature

Symbol	Description
$\boldsymbol{\sigma}$	Flow stress
$\boldsymbol{\varepsilon}$	Strain
$\boldsymbol{T}$	Temperature
$\dot{\boldsymbol{\varepsilon}}$	Strain rate
$\dot{\boldsymbol{\varepsilon}}^*$	Dimensionless strain rate $\dot{\varepsilon}^* = \dot{\varepsilon}/\dot{\varepsilon}_r$
$\boldsymbol{T}^*$	Homologous temperature: $T^* = (T - T_r)/(T_m - T_r)$
$\boldsymbol{T_r}$	The temperature at the reference condition: $T_r = 673\ K$
$\dot{\boldsymbol{\varepsilon}}_{\boldsymbol{r}}$	The strain rate at the reference condition: $\dot{\varepsilon}_r = 0.001\ s^{-1}$.
$\boldsymbol{Q}$	The activation energy
$\boldsymbol{Z}$	Zener-Hollomon parameter

5. References

[1] L. Chen, G. Zhao, J. Yu, Hot deformation behavior and constitutive modeling of homogenized 6026 aluminum alloy, *Materials & Design*, 74 (2015) 25-35.

[2] G.R. Johnson, W.H. Cook, A Constitutive model and data for materials subjected to large strains, high strain rates, and high temperatures, 7th International Symposium on Ballistics, The Hague, Netherlands, 1983, pp. 541-547.

[3] B. Ke, L. Ye, J. Tang, Y. Zhang, S. Liu, H. Lin, Y. Dong, X. Liu, Hot deformation behavior and 3D processing maps of AA7020 aluminum alloy, *Journal of Alloys and Compounds*, 845 (2020) 156113.

[4] Q.S. Dai, Y.L. Deng, J.G. Tang, Y. Wang, Deformation characteristics and strain-compensated constitutive equation for AA5083 aluminum alloy under hot compression, *Transactions of Nonferrous Metals Society of China*, 29(11) (2019) 2252-2261.

[5] X. Qian, N. Parson, X.G. Chen, Effects of Mn addition and related Mn-containing dispersoids on the hot deformation behavior of 6082 aluminum alloys, *Materials Science and Engineering: A*, 764 (2019) 138253.

[6] J. He, J. Wen, X. Zhou, Y. Liu, Hot deformation behavior and processing map of cast 5052 aluminum alloy, *Procedia Manufacturing*, 37 (2019) 2-7.

[7] Y. Sun, Z. Cao, Z. Wan, L. Hu, W. Ye, N. Li, C. Fan, 3D processing map and hot deformation behavior of 6A02 aluminum alloy, *Journal of Alloys and Compounds*, 742 (2018) 356-368.

[8] L. Chen, G. Zhao, J. Yu, W. Zhang, Constitutive analysis of homogenized 7005 aluminum alloy at evaluated temperature for extrusion process, *Materials & Design (1980-2015)*, 66 (2015) 129-136.

[9] Z. Wang, A. Wang, J. Xie, Dynamic softening mechanism of 2 vol.% nano-sized SiC particle reinforced Al-12Si matrix composites during hot deformation, *Materials Research Express*, 7(8) (2020) 086520.

[10] X. Chen, D. Fu, J. Teng, H. Zhang, Hot deformation behavior and mechanism of hybrid aluminum-matrix composites reinforced with micro-SiC and nano-TiB_2, *Journal of Alloys and Compounds*, 753 (2018) 566-575.

[11] S. Narayan, A. Rajeshkannan, Studies on formability of sintered aluminum composites during hot deformation using strain hardening parameters, *Journal of Materials Research and Technology*, 6(2) (2017) 101-107.

[12] S.J. Yii, N.M. Anas, M.N. Ramdziah, A.S. Anasyida, Microstructural and mechanical properties of Al-20%Si containing cerium, *Procedia Chemistry*, 19 (2016) 304-310.

[13] Y. Song, A. Wang, D. Ma, J. Xie, Z. Wang, P. Liu, Hot-deformation behavior and microstructure evolution of the dual-scale SiCp/A356 composites based on optimal hot-processing parameters, *Materials*, 13(12) (2020) 2825.

[14] X. Xia, H.J. McQueen, Deformation behaviour and microstructure of a 20% Al_2O_3 reinforced 6061 Al composite, *Applied Composite Materials*, 4(6) (1997) 333-347.

[15] X. Kai, Y. Zhao, A. Wang, C. Wang, Z. Mao, Hot deformation behavior of in situ nano ZrB_2 reinforced 2024Al matrix composite, *Composites Science and Technology*, 116 (2015) 1-8.

[16] P. Zhang, W. Zhang, Y. Du, Y. Wang, High-performance Al-1.5 wt% Si-Al_2O_3 composite by vortex-free high-speed stir casting, *Journal of Manufacturing Processes*, 56 (2020) 1126-1135.

[17] K.S. Lakshmi Narayana, M.M. Benal, H.K. Shivanand, Effect of graphite on aluminium matrix composites fabricated by stir casting route–A review, *Materials Today: Proceedings*, 45 (2021) 327-331.

[18] K.V. Prasad, K.R. Jayadevan, Simulation of stirring in stir casting, *Procedia Technology*, 24 (2016) 356-363.

[19] Y.C. Lin, X.M. Chen, A critical review of experimental results and constitutive descriptions for metals and alloys in hot working, *Materials & Design*, 32(4) (2011) 1733-1759.

[20] H. Mirzadeh, Constitutive modeling and prediction of hot deformation flow stress under dynamic recrystallization conditions, *Mechanics of Materials*, 85 (2015) 66-79.

[21] G.Z. Quan, Y.P. Mao, G.S. Li, W.Q. Lv, Y. Wang, J. Zhou, A characterization for the dynamic recrystallization kinetics of as-extruded 7075 aluminum alloy based on true stress–strain curves, *Computational Materials Science*, 55 (2012) 65-72.

[22] Y.C. Lin, X.M. Chen, G. Liu, A modified Johnson–Cook model for tensile behaviors of typical high-strength alloy steel, *Materials Science and Engineering: A*, 527(26) (2010) 6980-6986.

[23] D. Samantaray, S. Mandal, A.K. Bhaduri, A comparative study on Johnson-Cook, modified Zerilli-Armstrong and Arrhenius-type constitutive models to predict elevated temperature flow behaviour in modified 9Cr-1Mo steel, *Computational Materials Science*, 47(2) (2009) 568-576.

[24] A. He, G. Xie, H. Zhang, X. Wang, A comparative study on Johnson–Cook, modified Johnson–Cook and Arrhenius-type constitutive models to predict the high temperature flow stress in 20CrMo alloy steel, *Materials & Design (1980-2015)*, 52 (2013) 677-685.

[25] Y. Deng, Z. Yin, J. Huang, Hot deformation behavior and microstructural evolution of homogenized 7050 aluminum alloy during compression at elevated temperature, *Materials Science and Engineering: A*, 528(3) (2011) 1780-1786.

[26] N. Jin, H. Zhang, Y. Han, W. Wu, J. Chen, Hot deformation behavior of 7150 aluminum alloy during compression at elevated temperature, *Materials Characterization*, 60(6) (2009) 530-536.